論文 / 著書情報
Article / Book Information

Title	Spreading dynamics associated with transient solidification of a paraffin droplet impacting a solid surface
Authors	Chao Kang, Ikki Ikeda, Motoki Sakaguchi
Citation	International Journal of Heat and Mass Transfer, Vol. 228, , 125672
Pub. date	2024, 5
DOI	https://dx.doi.org/10.1016/j.ijheatmasstransfer.2024.125672

International Journal of Heat and Mass Transfer 228 (2024) 125672

Contents lists available at ScienceDirect

International Journal of Heat and Mass Transfer

journal homepage: www.elsevier.com/locate/ijhmt

Spreading dynamics associated with transient solidification of a paraffin droplet impacting a solid surface

Chao Kang, Ikki Ikeda, Motoki Sakaguchi *

Department of Mechanical Engineering, Tokyo Institute of Technology, 2-12-1, Ookayama, Meguro-ku, Tokyo 152-8552, Japan

ARTICLE INFO

Keywords:
Droplet impact
Spreading dynamics
Splat solidification
Paraffin wax
Transparent substrates

ABSTRACT

The solidification of a droplet after impacting a solid substrate initiates immediately at the bottom surface owing to rapid heat transfer. Transient splat solidification greatly affects the spreading dynamics, such as flattening and recoil. This study experimentally and numerically studied the spreading and transient solidification of a paraffin droplet impacting transparent solid substrates. The impact phenomena, including flattening, recoil, final splat geometry, and solidification at the bottom surface, were observed using a high-speed camera from the side and bottom. The effects of the substrate material, substrate temperatures, and droplet temperatures were thoroughly discussed. The results suggest that there are two patterns of splat solidification, depending on the impact conditions. The impacted droplet (with a temperature of 123 °C) started to solidify at the periphery and gradually progressed toward the splat center on low-thermal-conductivity polycarbonate substrates. For lower initial droplet temperatures or substrates with higher thermal conductivity, solidification occurred immediately after the impact across the entire bottom surface of the splat owing to the faster cooling. Numerical simulations were performed to reproduce the impact phenomena and good agreement was obtained for the spreading factor, recoil height, final splat geometry, and solidification at the bottom surface of the splats. An in-depth comparison between the experimental and simulation results revealed that the transient solidification immediately after impact significantly affected the spreading of the impacted droplets, especially when the substrate had a high thermal conductivity. The results demonstrate that the proposed experimental and numerical methods provide accurate evaluation and prediction of droplet impact, concerning transient solidification and its influence on the spreading dynamics of the droplets.

1. Introduction

The spreading and solidification of an impacted droplet on a solid surface is a common phenomenon in various industrial sectors, including thermal spraying [1], inkjet printing [2], droplet-based additive manufacturing [3], and airframe icing [4]. Because the outcomes of droplet impact play key roles in the performance of the related components and products, this topic of research has attracted engineers and scientists from various fields. Depending on the specific applications, various impact behaviors have been thoroughly studied [5]. Within the field of fluid mechanics, the main focus has been on flattening [6], splashing [7], recoil and rebound [8], and boiling [9] of the impacted droplets. In the field of solid mechanics, the thermal stress [10,11], adhesion [12–14], and cracking [15] of solidified splats have been frequently studied.

Splat solidification occurs during the phase transition from liquid to solid, and is associated with heat transfer with solid surfaces and ambient air. The solidification usually initiates at the bottom immediately after the impact along with the spreading of the liquid [16]. The solid layer at the bottom surface of the impacted droplet strongly affects the impact behavior owing to the high local viscosity. Therefore, it is important to understand the mechanism of transient solidification immediately after impact to achieve a better understanding and more precise prediction of droplet-impact phenomena.

Numerical simulations [16–22] have been widely used to study the solidification of impacted droplets. For example, Kang et al. [16] modeled the impact and solidification of a paraffin droplet on a metal substrate. The geometry of the solidified splat was numerically calculated and the simulation results showed good agreement with the experimental measurements. Fukudome et al. [17] simulated the solidification phenomena of a molten Sn droplet impacting a substrate using an explicit moving-particle simulation method. They found that

* Corresponding author.
E-mail address: sakaguchi.m.ac@m.titech.ac.jp (M. Sakaguchi).

https://doi.org/10.1016/j.ijheatmasstransfer.2024.125672
Received 27 February 2024; Received in revised form 11 April 2024; Accepted 5 May 2024

the solidification timescale for splats depends on the local film thickness. The solidification on the outer surface starts at the thin periphery and progresses toward the thick center. Bot et al. [20] studied the thermal-spraying process by simulating the impact and solidification of ceramic droplets. An Eulerian–Lagrangian approach was used to track the droplet/gas interface and the liquid/solid front during splat solidification. They considered the interactions of neighboring splats and investigated the formation of gas traps and the effects on the coating properties. Zhang et al. [22] focused on the interactions between neighboring droplets, and their results suggested that the solidification of the second droplet determined interface bonding and splat morphologies. Most of the previous studies focused on the general solid behavior and the geometry of fully solidified splats. Few researchers have studied the mechanism of the initiation of solidification at the interface, which has a significant effect on the subsequent spreading dynamics. Several works [23–27] have observed the solidification of impacted droplets on solid substrates. Fang et al. [28,29] experimentally investigated the coupling effect between the drop-scale fluid dynamics and splat solidification by impacting a water droplet with a subcooled surface with special consideration of the effect of the inclined angle of substrates. Previous results generally reported the final splat geometry or the time evolution of the solidification along the thickness direction. To fully understand the mechanism of solidification at the splat/substrate interface, it is necessary to directly investigate the transient solidification at the bottom surface of the splat.

Recently, transparent substrates have been used to carry out droplet-impact tests to study gas traps [30], vapor film at the interface [31], and boiling on superheated substrates [32] by observing the bottom surface of the impacted droplet. Transparent substrates have advantages over solid substrates, such as metals, because they allow direct observations of the splat/substrate interface. In this work, droplet impact was observed on three types of transparent substrate using a high-speed camera to study the transient solidification of the impacted droplets and their spreading dynamics. Special consideration was given to the effects of the substrate material, droplet temperature, and substrate temperature. Numerical simulations were carried out to quantitatively reproduce the experimental results, including the spreading factor, recoil height, final splat geometry, and transient solidification at the interface.

2. Droplet-impact experiments

2.1. Testing setup

The setup for the droplet-impact tests was modified from setups used in previous studies [16,33] and is sketched in Fig. 1. The droplet was generated and free-fell onto a solid substrate. The impact and solidification of the droplet were observed using a high-speed camera (HAS-D71, DITECT Co., Ltd.). An industrial paraffin wax (HNP-9, Nippon Seiro, Japan) with a melting point of approximately 80°C was selected as the droplet material because it can be easily melted and solidified near room temperature. The paraffin wax was pre-melted in a heated aluminum holder, into the bottom on which a needle with a 3.0-mm inner diameter was inserted. Droplets could be generated at the needle tip by turning up the micrometer head (MHH2-50, Mitutoyo). Droplets detached from the needle and impacted the substrate when their weight exceeded the surface tension force. For a given paraffin wax, the mass of each droplet is constant for a given droplet temperature, which was controlled by a thermocouple (Type K, 0.32-mm wire diameter) attached to the bottom of the holder.

Droplet-impact tests were conducted under isothermal and non-isothermal conditions. In the isothermal impact tests, the substrate was placed onto a hot aluminum block. The substrate temperature was kept the same as the droplet temperature using a hot plate placed beneath the aluminum block. No cooling and solidification of the impacted droplet took place during the tests. A high-speed camera was used to capture the horizontal view of the impact behaviors, as shown in Fig. 1. In the non-isothermal impact tests, the initial temperature of the substrate was controlled at approximately 20 °C using an air conditioner. The impacted droplet cooled and solidified on the substrate, which involved heat transfer from the droplet to the substrate. In both the isothermal and non-isothermal impact tests, the heat of the droplet slightly dissipated to the environment owing to convective and radiative heat transfer. In addition to horizontal observation, the splat/substrate interface was observed through the transparent solid substrates that were specifically used for photography from the bottom. As illustrated in Fig. 1, a hole was manufactured on the support stage and a 45 ° tilted mirror was equipped under the stage. A ring light was equipped to improve the brightness of the horizontal view. An extra ring light was placed over the hole for the bottom observation in the non-isothermal impact tests.

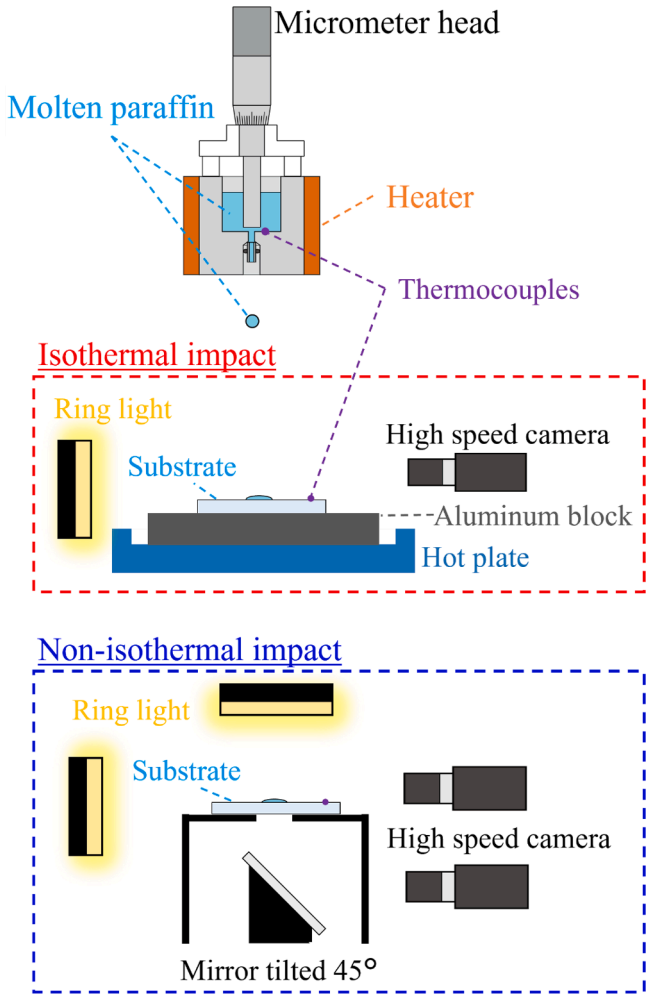

Fig. 1. Illustration of the setup for the droplet-impact tests. For the non-isothermal impact, a mirror was placed below the transparent substrate to observe the bottom surface of the impacted droplet with a high-speed camera.

2.2. Materials and experimental conditions

Three types of transparent material — polycarbonate, quartz glass, and sapphire glass — were used as substrates. The dimensions and surface roughness of each disc substrate are summarized in Table 1. Some of the main thermal and physical properties of the substrates are summarized in Table 2. The sapphire glass had the highest thermal conductivity, which is comparable to that of steels. The polycarbonate had the lowest thermal conductivity of 0.19 W/(m·K), which is close to

Table 1
Dimensions and surface roughness of the disc substrates.

Substrate material	Polycarbonate	Quartz glass	Sapphire glass
Diameter (mm)	40	40	40
Thickness (mm)	20	10	10
Surface roughness, Ra (nm)	23	6.8	4.4

Table 2
Thermal and physical properties of the substrates.

Substrate material	Polycarbonate	Quartz glass	Sapphire glass
Density (kg/m^3)	1200	2200	3980
Specific heat at 100 ℃ (J/(kg·K))	1260	749	750
Thermal conductivity at 20 ℃ (W/(m·K))	0.19	1.38	42
Thermal conductivity at 100 ℃ (W/(m·K))	–	–	25
Static contact angle at 95 ℃ (°)	11.5	15.8	14.5

that of paraffin wax. The material properties of paraffin wax (HNP-9), which have been extensively evaluated previously [10,13,16,34], are summarized in Table 3.

Three experimental variables were examined in this study: the substrate material, droplet temperature, and substrate temperature. Droplet temperatures were set at either 100 or 140 °C. The substrate temperature was 20 °C for non-isothermal impact tests and was set equal to the droplet temperature for the isothermal impact tests. Three aforementioned transparent substrates were tested for each droplet temperature and substrate temperature. A total of 12 experimental conditions (Table 4) were used to study the effects of the three experimental variables on the impact behavior. It should be noted that the droplet temperatures of 100 °C and 140 °C were the measured temperatures of the paraffin wax using a thermocouple attached to the aluminum holder (Fig. 1). The actual temperatures at the moment of impact were measured using a thermography camera. It was found that the temperatures decreased from 100 and 140 °C to 95 and 123 °C, respectively. These actual values at the impact were treated as the droplet temperatures in the following analysis. The Weber numbers were 129 and 138 for droplet temperatures of 95 and 123 °C, respectively. The Reynolds numbers were 551 and 914 for droplet temperatures of 95 and 123 °C, respectively. A unique testing serial number was assigned to each test condition in Table 4. For example, test No. (2) P-123-20 represents test conditions of a polycarbonate substrate, droplet temperature of 123 °C, and substrate temperature of 20 °C. The height of the impact from the needle tip to the substrate surface was kept constant at 50 mm for all tests. The impact velocity was calculated as 0.99 m/s by assuming free-fall. Three tests were conducted for each testing condition.

Table 3
Thermal and physical properties of paraffin-wax droplets.

Material	Paraffin wax droplets
Density (liquid) (kg/m^3)	760
Density (solid) (kg/m^3)	930
Specific heat at 100 ℃ (J/(kg·K))	2300
Latent heat of solidification (J/kg)	1.9×10^5
Solidus temperature (℃)	65
Liquidus temperature (℃)	90
Thermal conductivity at 25 ℃ (W/(m·K))	0.26
Dynamic viscosity at 80 ℃ (Pa·s)	0.0076
Dynamic viscosity at 90 ℃ (Pa·s)	0.00616
Dynamic viscosity at 120 ℃ (Pa·s)	0.00380
Dynamic viscosity at 140 ℃ (Pa·s)	0.00296
Surface tension at 95 ℃ (N/m)	0.0217
Surface tension at 123 ℃ (N/m)	0.0194

Table 4
Droplet-impact conditions.

Testing No.	Substrate material	Droplet temperature	Substrate temperature
(1) P-123-123	Polycarbonate	123 °C	123 °C
(2) P-123-20	Polycarbonate	123 °C	20 °C
(3) P-95-95	Polycarbonate	95 °C	95 °C
(4) P-95-20	Polycarbonate	95 °C	20 °C
(5) Q-123-123	Quartz glass	123 °C	123 °C
(6) Q-123-20	Quartz glass	123 °C	20° C
(7) Q-95-95	Quartz glass	95 °C	95 °C
(8) Q-95-20	Quartz glass	95 °C	20 °C
(9) S-123-123	Sapphire glass	123 °C	123 °C
(10) S-123-20	Sapphire glass	123 °C	20 °C
(11) S-95-95	Sapphire glass	95 °C	95 °C
(12) S-95-20	Sapphire glass	95 °C	20 °C

3. Experimental results

3.1. Flattening, recoil, and final geometry

Horizontal views of the isothermal and non-isothermal droplet impacts during the initial 30 ms after the first contact with the substrate are shown in Figs. 2 and 3, respectively. The impact conditions were carefully selected to prevent splat splashing. As can be seen in the photographs, a microsatellite droplet fell onto the primary droplet at approximately 30 ms. Satellite droplets were undesirably generated when the droplets broke up and departed from the remaining liquid at the needle tip [35].

For all six isothermal impact conditions, the droplet flattened on the substrate until it reached the equilibrium state without any obvious recoil. Recoil could be observed for non-isothermal impact (Fig. 3). The extent of the recoil presented a clear correlation with the droplet temperature, with more intensive recoil and a larger peak recoil height occurring at the lower droplet temperature of 95 °C. The spreading factor, d/d_0, and dimensionless height, h/d_0, were used to quantify the impact behavior. Both d/d_0 and h/d_0 were calculated from the photographs in Figs. 2 and 3 following the rules described in Fig. 4. The evolutions of d/d_0 in the initial 25 ms and h/d_0 in the initial 50 ms are provided in Figs. 5 and 6, respectively. The average of three tests was plotted in Figs. 5 and 6 and following experimental results of d/d_0 and h/d_0. Error bars were also indicated in these figures, but they are very narrow in some cases due to the small variance in the measured spreading factors. The spreading factor became stable at approximately 10 ms with values ranging from 2 to 3.5. In Fig. 6, the recoil can be observed for non-isothermal impact, where a peak dimensionless height h/d_0 appeared at 20–25 ms. According to the numerical simulations described in Section 4, under non-isothermal conditions, the splat gradually solidified on the substrate within 5 to 15 s depending on the droplet temperature and substrate material. The final geometries of the splats after solidification were measured using a stylus-type surface profiler (DSF600K31, Kosaka Laboratory Ltd., Tokyo, Japan). The splat geometries are summarized in Fig. 7 for droplet temperatures of (a) 95 °C and (b) 123 °C. Generally, a thicker splat with a narrower diameter was observed at a lower droplet temperature and on a high-thermal-conductivity substrate.

3.2. Transient solidification at the bottom surface

Solidification of the impacted droplet initiated at the bottom surface owing to rapid heat transfer with the substrate. The time evolutions of splat solidification at the bottom surface were photographed through the transparent substrates for all six non-isothermal impacts, as shown in Fig. 8. The splats were black before solidification. They gradually changed to white as they solidified because of the scattering of the ring

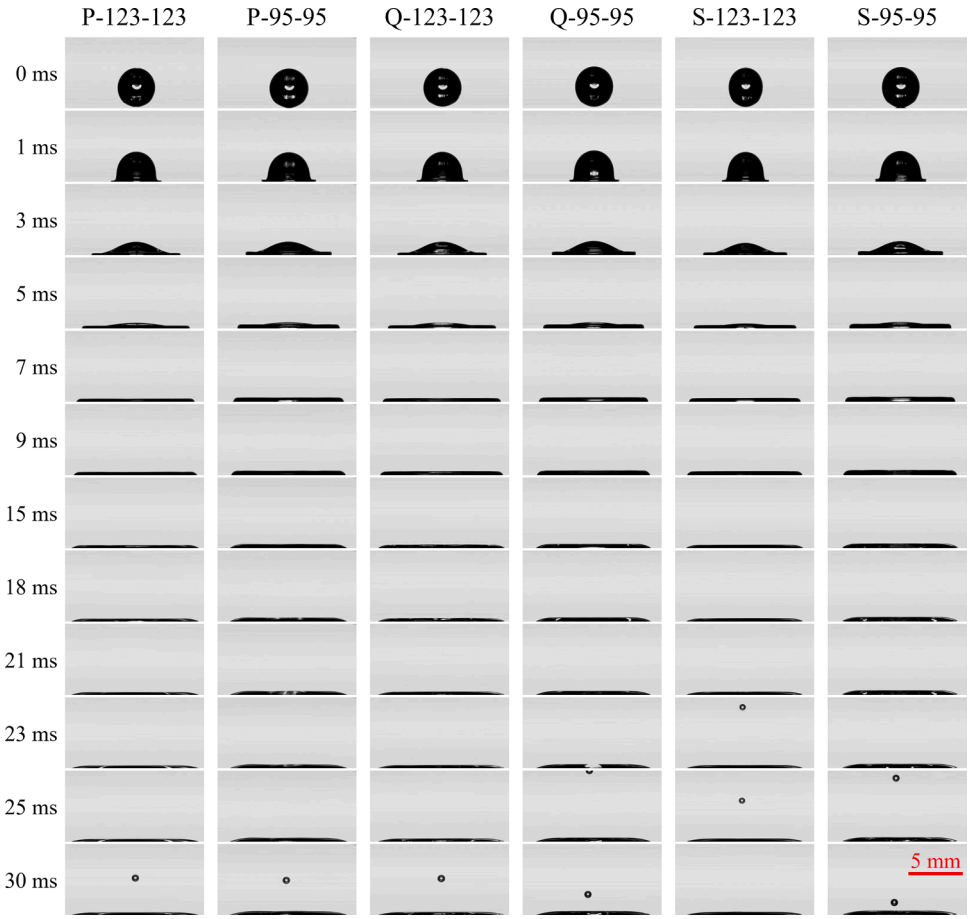

Fig. 2. Horizontal view of isothermal impact during the initial 30 ms.

light at the solidified area. In other words, a larger gray value represents a higher degree of solidification. It should be noted that a white ring can be seen near the splat periphery in some photographs. This undesirable white ring does not indicate solidification and is formed by refraction of the piling up of the liquid near the splat edge (Fig. 3). Two types of solidification pattern were observed in Fig. 8 depending on the impact conditions. When the 123 °C droplets impacted the polycarbonate substrate (P-123-20 in Fig. 8), solidification started at approximately 500 ms and gradually propagated from the periphery to the splat center. For the other impact conditions, the solidification occurred immediately after impact and was initiated simultaneously across the entire bottom surface of the splat.

The evolutions of the gray values at the splat center were extracted from each photograph and plotted in Fig. 9 for droplet temperatures of (a) 123 °C and (b) 95 °C. The gray values increased as the solidification of the splat proceeded. A sharp reduction in the gray values occurred at approximately 25 ms under certain conditions. This was caused by the refraction at the splat center during recoil when the liquid flowed back from the periphery to the center. The refraction at the outer surface of the splat partly prevented the light from arriving at the center of its bottom surface, and hence led to a reduction of the gray value. The gray values gradually became saturated at approximately 215 for all conditions. This process took 10–10^3 ms depending on the impact conditions. Because the impacted droplets completely solidified after 5–15 s, saturation of the gray values occurred much earlier than the complete solidification of impacted droplets. In other words, the droplet is still in the liquid above the thin solid layer at the point of saturation of the gray values. For certain impact conditions, (e.g., S-95-20), the flow was still intense (Fig. 3) when the gray values reached saturation at approximately 10 ms. The transient solidification of the impacted droplet occurred within 10–10^3 ms, during which the gray values increased and reached saturation. The transient solidification is investigated by comparing the measured gray values and calculated solid-layer thickness in Section 5.

3.3. Effects of impact conditions

3.3.1. Effect of substrate temperature

The substrate temperatures were set as the droplet temperature for the isothermal impact tests and 20 °C for the non-isothermal impact tests. For isothermal impact, the splat spread on the substrate until the surface tension reached equilibrium at the contact point of the droplet, substrate, and air. Because the impacted droplet continued to move outward and flatten, no clear recoil occurred (Fig. 2). Under non-isothermal conditions, the droplet solidified near the interface immediately after impact. The flattening of the impacted droplet was greatly restricted owing to the rapid increase in the viscosity of the splat near the interface. In our previous study, liquid paraffin wax above the solidified layer was pulled back to the center by the surface tension force, which induced a recoil [16].

3.3.2. Effect of the substrate material

In this study, the substrate materials affected the impact behavior, mainly because of differences in their thermal conductivity, which was the lowest for polycarbonate and highest for sapphire glass (Table 2). Low thermal conductivity leads to slower heat transfer from the droplet to the substrate and hence results in a lower cooling rate and slower solidification. Without heat transfer and solidification, the substrate material has no obvious effect on isothermal impact behavior. Even though small differences in the static contact angle were measured for

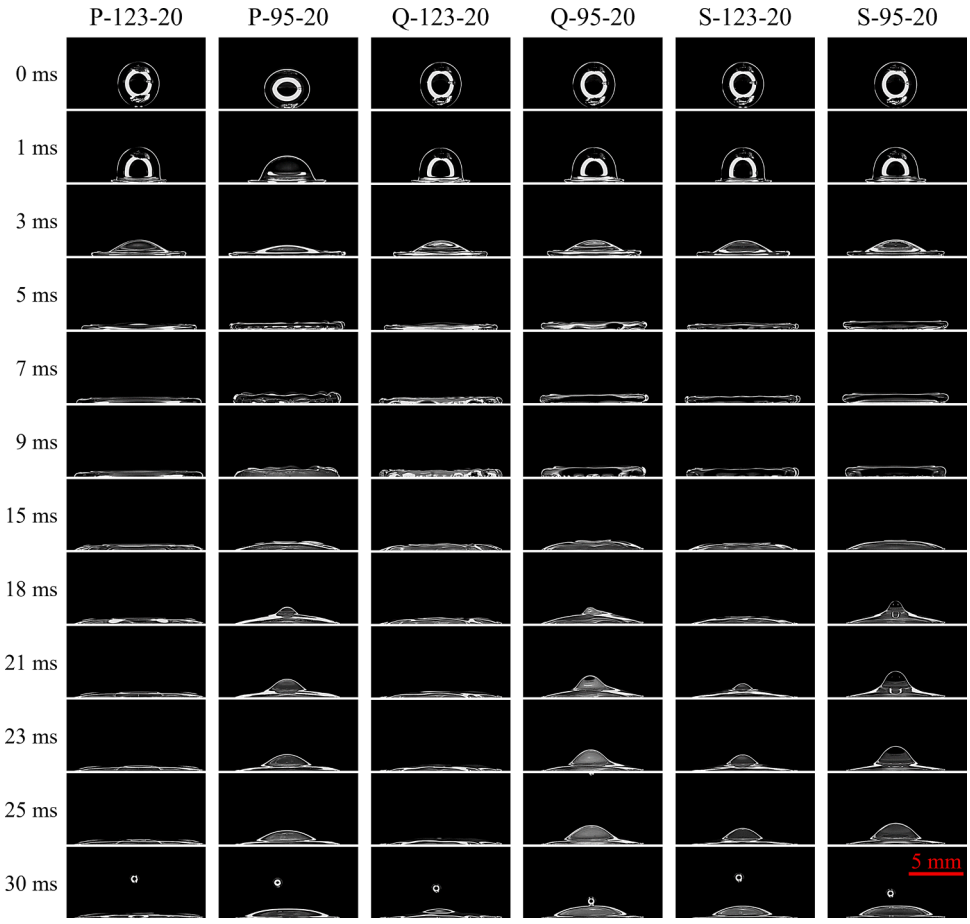

Fig. 3. Horizontal view of non-isothermal impact during the initial 30 ms.

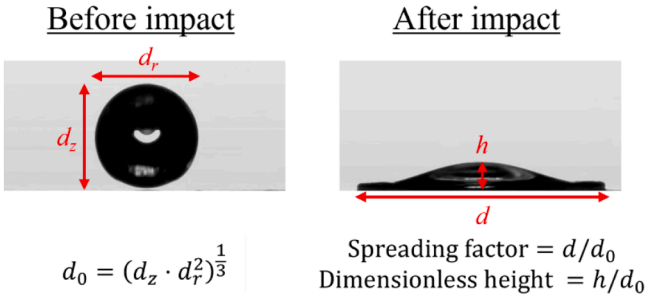

Fig. 4. Definitions of the spreading factor and dimensionless height.

the different substrates (Table 2), this had a limited effect on the spreading factor and recoil height (Figs. 5 and 6). The surfaces of three types of substrates are sufficiently smooth (*Ra* is less than 30 nm), thus, the effect of the surface roughness on spreading dynamics appears to be negligible.

For non-isothermal impact, the faster heat transfer with the sapphire-glass substrate caused faster solidification of the splat and resulted in a smaller spreading factor at the steady state (Fig. 5). A more-intense recoil with a larger peak height was also observed for the sapphire-glass substrate. This is because the smaller spreading factor suppressed the loss of kinetic energy of the liquid droplet during its viscous dissipation. As a result, the smallest diameter and largest thickness of the solidified splats were measured for the sapphire-glass substrate (Fig. 7).

Transient solidification at the bottom surface of the splat is another important phenomenon that can be affected by the substrate material. As stated in Section 3.2, when the 123 °C droplet impacted the polycarbonate substrate, the solidification started at 500 ms at the periphery and progressed to the center of the splat. For the quartz-glass and sapphire-glass substrates, solidification occurred much earlier and more quickly owing to rapid cooling at the interface. The lower thermal conductivity of the polycarbonate resulted in a much longer time to cool and solidify the impacted droplets.

3.3.3. *Effect of droplet temperature*

The impact behavior depends on the initial droplet temperature mainly because of the temperature dependence of the droplet viscosity and the difference between the initial temperature and the melting point. Higher droplet temperatures led to larger spreading factors mainly because of the lower viscosity for all impact tests (Fig. 5). For non-isothermal impact, lower peak recoil heights were measured for the higher droplet temperature because of the larger spreading factors (Fig. 6). As a result, thinner splats with larger diameters were measured for higher droplet temperatures as shown in Fig. 7. The droplet temperature also affected the solidification immediately after impact. As shown in Fig. 8, for a temperature of 123 °C, the splat solidified on the polycarbonate substrate from the periphery to the splat center and the interface was completely solidified at approximately 1500 ms. At 95 °C, the splat solidified at the interface much more quickly (within 50 ms). In addition, the solidification took place simultaneously across the entire bottom surface owing to the smaller difference between the initial temperature and the melting point.

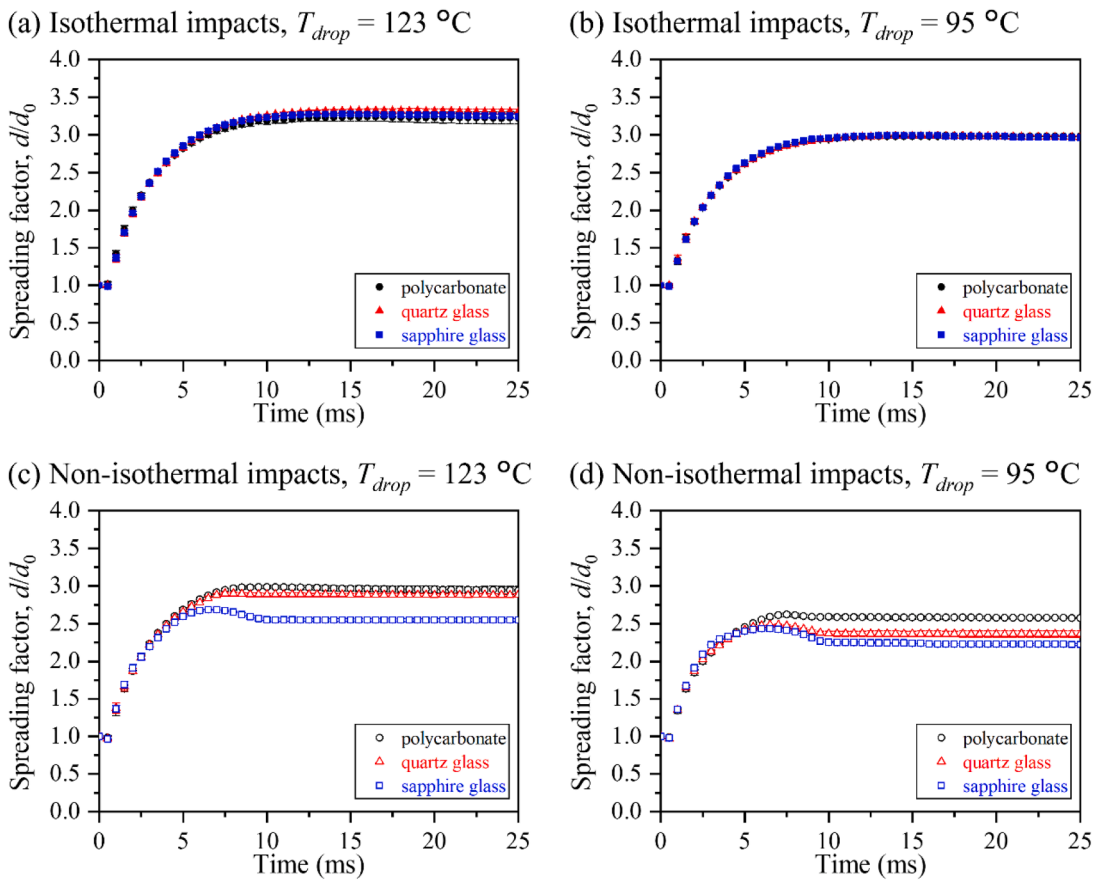

Fig. 5. Experimental results of the time evolutions of the spreading factor.

4. Numerical simulation

4.1. Simulation model

A typical numerical model and mesh distribution are sketched in Fig. 10. The droplet was assumed to have a spherical shape before impact. The diameters were calculated according to the mass and density as 3.74 and 3.60 mm for droplet temperatures of 95 and 123 °C, respectively. The impact and solidification of the droplet induced by transient heat transfer with the substrate and environment were calculated for all impact conditions. The environmental temperature, pressure, and heat-transfer coefficient were set as 20 °C, 1 atm, and 10 W/(m^2·K), respectively. The temperature-dependent surface tension and static contact angle (see Table 2) were measured and incorporated to account for the surface wettability during impact. The dynamic contact angle was not used in our work because the droplet spreading dynamics were dominated by the high wettability and rapid solidification in the current impact tests. Considering the well-interfacial contact resulting from the smooth substrate surfaces and low impact temperature, the interfacial thermal contact resistance was neglected in the simulation. However, it should be noted that the absence of dynamic contact angle and contact thermal resistance could lead to minor simulation errors. Particularly in the case of widely studied water droplet impact, significant simulation errors might arise if the dynamic contact angle is not considered.

Commercial software FLOW-3D (Flow Science, Inc.) was used to model the impact and solidification of the paraffin droplet using an axis-symmetric model. Finite-difference approximations were used to solve the Navier–Strokes equations. The finite-volume method was used to ensure the conservation of fluxes on each grid and the whole domain. Conservations of mass, momentum, and energy can be described using the following equations:

$$\nabla\cdot\mathbf{u} = 0, \tag{1}$$

$$\rho\frac{\partial\mathbf{u}}{\partial t} + \rho\nabla\cdot(\mathbf{uu}) = -\nabla P + \mathbf{f} + \rho\mathbf{g} + \rho\mathbf{F} + \mathbf{S}, \tag{2}$$

$$\rho\frac{\partial I}{\partial t} + \rho\nabla\cdot(\mathbf{u}I) = -P\nabla\cdot\mathbf{u} + \nabla\cdot(k\nabla T) + h(T_{\text{wall}} - T), \tag{3}$$

where t is the time, ρ is the density, $\mathbf{u}$ is the velocity vector, P is the pressure, $\mathbf{f}$ is a viscosity term, $\mathbf{g}$ is the gravitational body acceleration, $\mathbf{F}$ is a source term owing to solidification, which can be described by Eq. (7) (Section 4.2), $\mathbf{S}$ is a surface-tension term, k is the thermal conductivity, h is the heat transfer coefficient, T and T_{wall} are the temperatures of the liquid and wall, respectively, and I is the internal energy, which can be described by

$$I = cT + (1 - f_s)L, \tag{4}$$

where c and L are the specific heat and latent heat, respectively, and f_s is the solid fraction, which is a function of local temperature. The volume-of-fluid method [36] was used to track the free surface, where a fractional parameter, F, was used to identify the status of each calculation element. F has a value ranging from 0 to 1, representing the fluid fraction of each element. To track the interface between the liquid and the ambient air, the continuity equation was solved:

$$\frac{\partial F}{\partial t} + \mathbf{u}\cdot\nabla F = 0. \tag{5}$$

More-detailed descriptions of the simulation model can be found in our previous work [16].

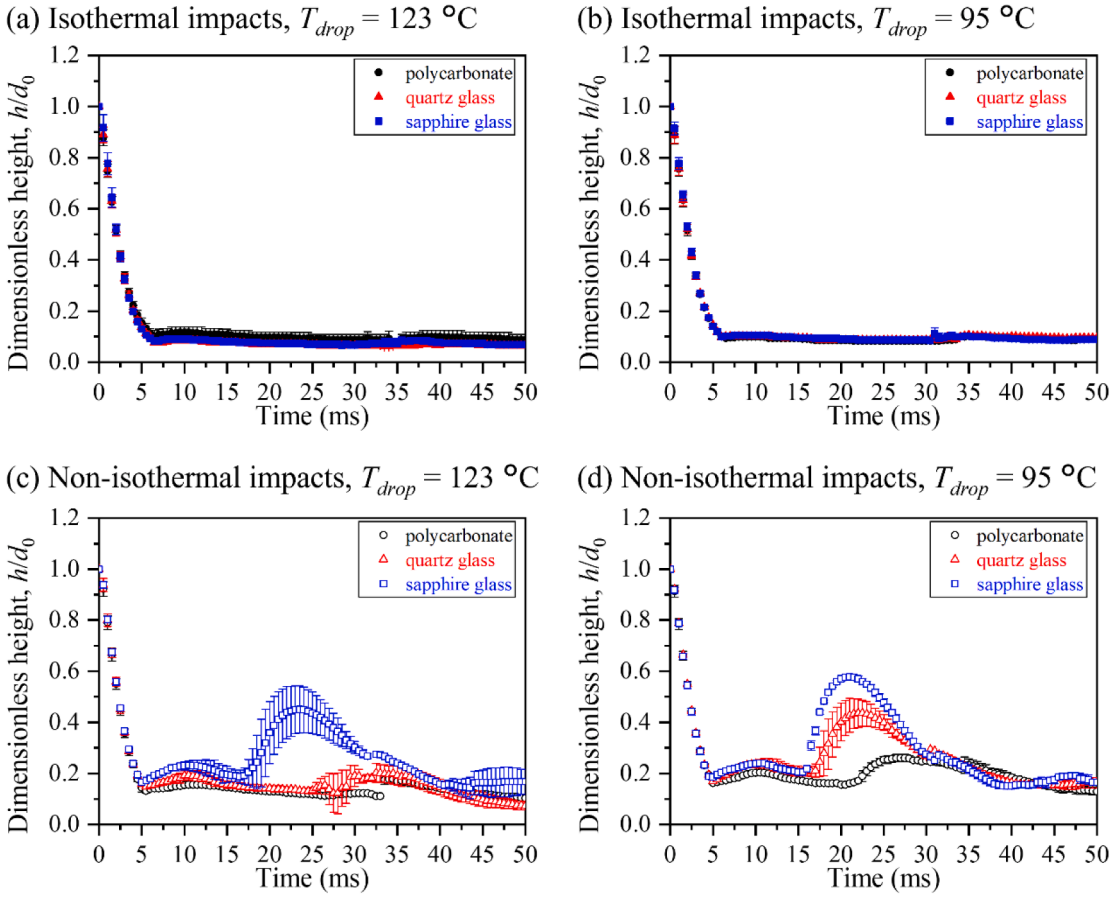

Fig. 6. Experimental results of the time evolution of the dimensionless height.

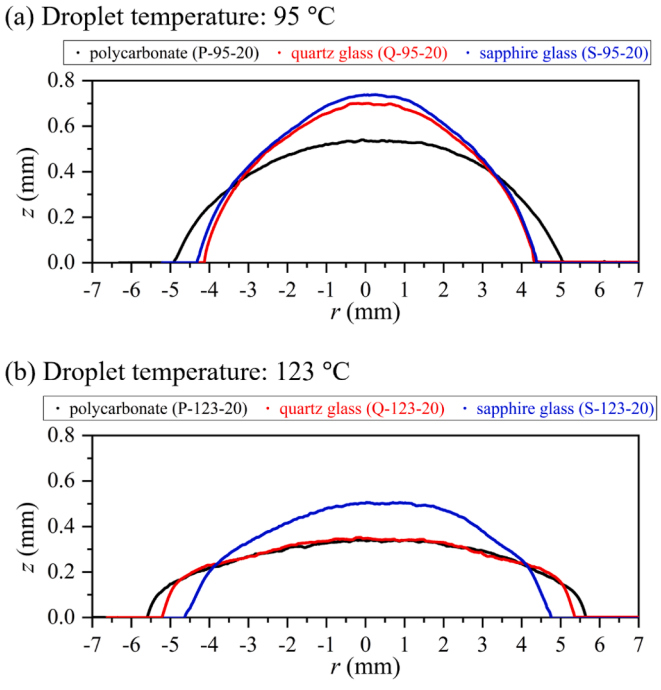

Fig. 7. Final geometries of the solidified splats under non-isothermal impact for droplet temperatures of (a) 95 °C and (b) 123 °C.

4.2. Numerical considerations of the splat solidification

Paraffin wax is a non-crystalline material that melts over a range of temperatures. The solidification of the droplet was determined by the local temperature. A solid fraction, f_s, was assigned to each element according to its temperature, following the relationship shown in Fig. 11 (b), which was calculated using Eq. 6 based on differential scanning calorimetry measurements during phase transition (Fig. 11(a)):

$$f_s(T) = \frac{\int_T^{T_l} (c(T) - c_{base})dT}{\int_{T_s}^{T_l} (c(T) - c_{base})dT}, \tag{6}$$

where, T_s and T_l are the solidus and liquidus temperatures, respectively, c is the specific heat, and c_{base} is the baseline for calculating the latent heat during phase transition. The effect of solidification on the fluid flow is considered in the momentum equation via the momentum source term **F**,

$$\mathbf{F} = -\mathrm{TSDRG}\frac{f_s^2}{(1-f_s)^3}\mathbf{u}. \tag{7}$$

TSDRG is a constant that depends on the mushy-zone microstructure [16]. The values of TSDRG were calculated as 1.32×10^9 and 8.7×10^8 s^{-1} for droplet temperatures of 95 and 123 °C, respectively.

4.3. Mesh sensitivity analysis

The accuracy of the simulation generally increases with a reduction of the mesh size. However, precise modeling of the current impact and spreading behavior requires a large amount of computing resources, particularly for non-isothermal impact. Therefore, mesh sensitivity

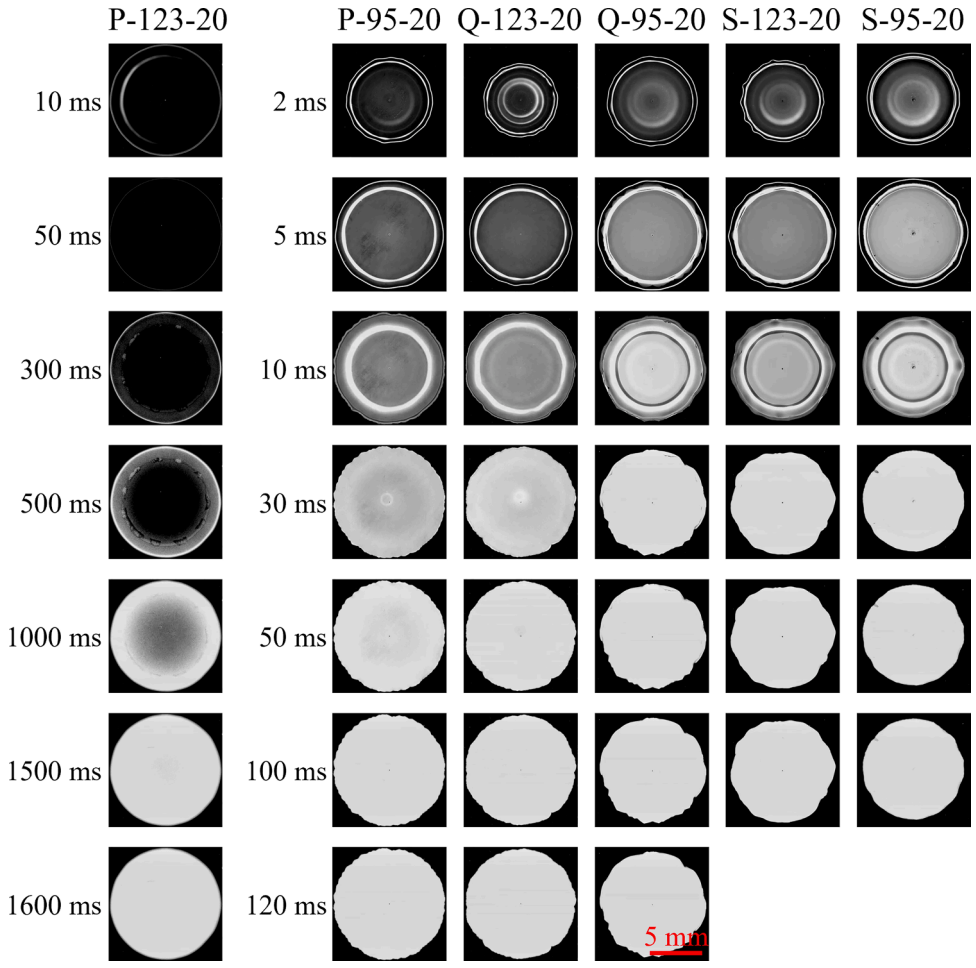

Fig. 8. Photographs at the bottom surface of impacted splats. The splat changed from black to white during solidification.

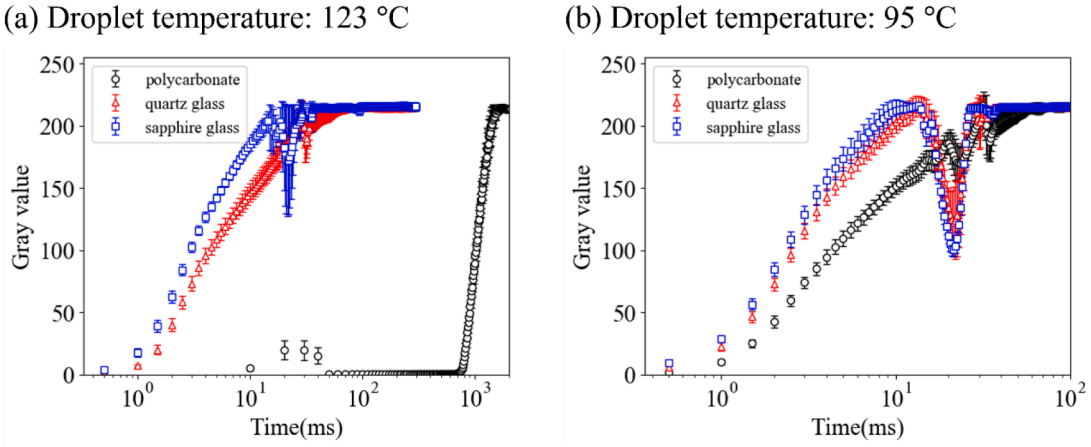

Fig. 9. Time evolutions of the gray values at the center of the bottom surface of the splat under non-isothermal impact for droplet temperatures of (a) 123 °C and (b) 95 °C.

analysis was performed to find the most-efficient mesh distributions. Considering the great importance of the mesh resolution at the interface, a fine mesh was applied to the interface to study the effect on the calculated spreading factor. Table 5 shows eight mesh distributions of the liquid domain tested in the sensitivity analysis. The mesh size for the substrate domain was fixed at 50 μm. The calculated spreading factors for the various mesh distributions of the liquid domain can be found in our previous study [16], where the simulation results became stable for interface mesh sizes of 2 and 5 μm for non-isothermal and isothermal impact, respectively. The mesh distributions of the liquid domain were therefore set as No. 4 and No. 6, as described in Table 5, for isothermal and non-isothermal impact, respectively.

The mesh size for the substrate affects the simulation results for non-isothermal impact by influencing the heat transfer at the interface and within the substrate, especially the rapid heat transfer immediately after impact. Quadrilateral substrate elements with sizes of 5, 10, 25, and 50

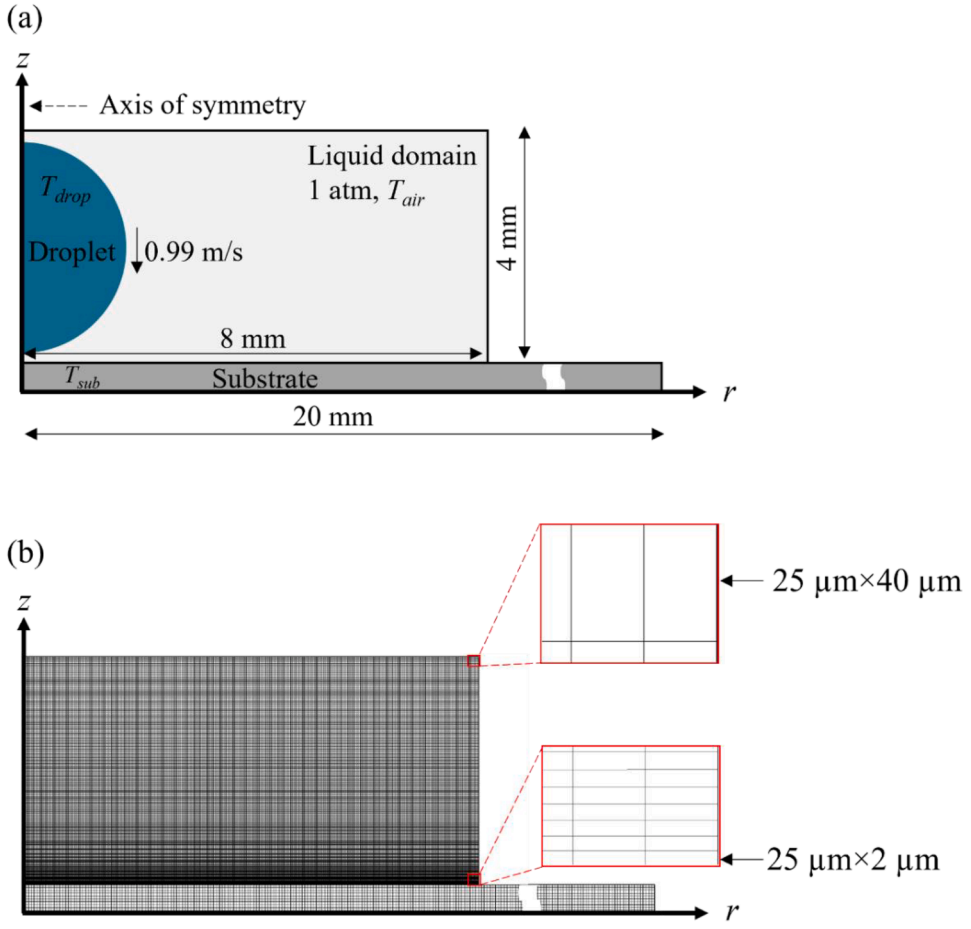

Fig. 10. (a) Axis-symmetrical numerical model and (b) a typical mesh distribution.

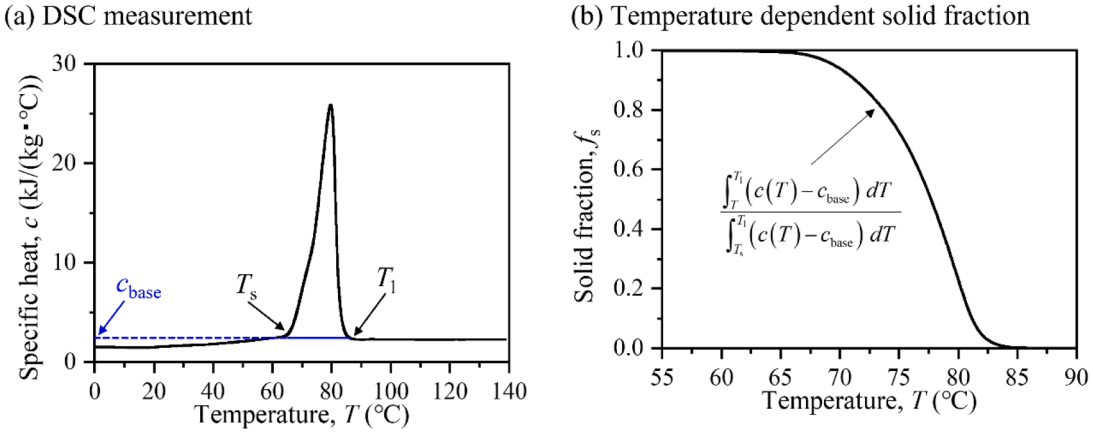

Fig. 11. (a) DSC measurement of the paraffin wax and (b) temperature-dependent local solid fraction.

μm were examined to investigate the effects on the calculated spreading factor. The mesh distribution for the liquid domain was fixed as No. 6 (Table 5), as determined by the former analysis. The calculated spreading factors for each type of substrate are shown in Fig. 12 for a droplet temperature of 95 °C. No clear difference could be seen for the sapphire-glass substrate with different substrate mesh sizes. The spreading factors decreased and approached the experimental values when the mesh sizes of the quartz-glass and polycarbonate substrates were reduced. This might be caused by their low thermal conductivities, which led to a large temperature gap at the interface, and a large temperature gradient within the substrate. Therefore, a finer mesh distribution is required to accurately calculate the heat transfer and spreading factor at the interface for substrates of polycarbonate and quartz glass. In Fig. 12, the spreading factors become stable at a substrate mesh size of 10 μm; this value was used in all non-isothermal simulations.

Table 5
Mesh distributions of the liquid domain to be examined (unit: μm).

No.	Mesh size along r-axis	Mesh size along z-axis (bottom surface)	Mesh size along z-axis (top surface)
1	80	80	80
2	40	40	40
3	25	10	40
4	25	5	40
5	25	3	40
6	25	2	40
7	25	1	40

5. Simulation results and discussion

5.1. Dynamic spreading and final geometry

Fig. 13 shows comparisons of the experimental and simulated time evolutions of splat geometries on sapphire glass under (a) isothermal and (b) non-isothermal conditions for a droplet temperature of 95 °C. Good agreement was achieved for key impact behaviors, including flattening and recoil. Fig. 14 shows the spreading factors in the initial 25 ms, in which the data points represent the experimental measurements and the curves represent the simulation results. High accuracy was achieved for simulations for both isothermal (Fig. 14(a, b)) and non-isothermal impact (Fig. 14(c, d)). The undesirably generated

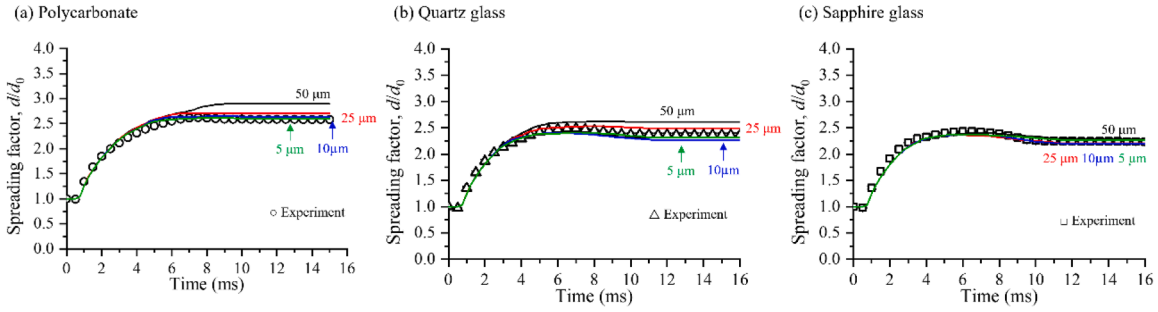

Fig. 12. Effect of the mesh size of the substrate on the spreading factors for (a) polycarbonate, (b) quartz-glass, and (c) sapphire-glass substrate materials. The droplet temperature is 95 °C.

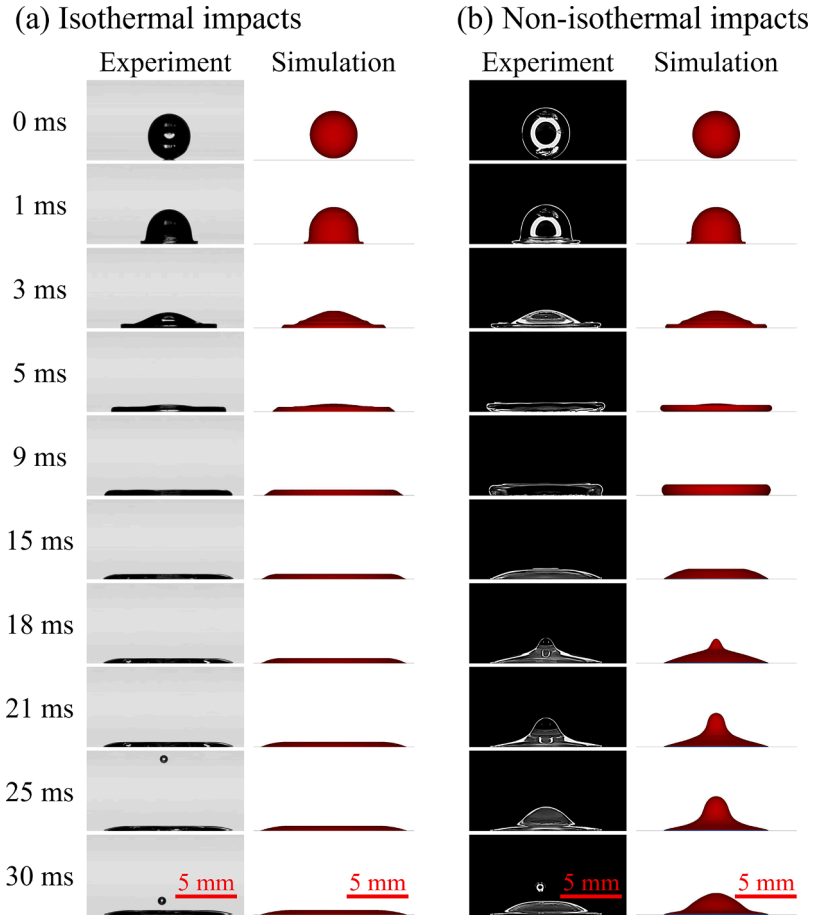

Fig. 13. Comparison of the experimental and simulated time evolutions of splat geometries under (a) isothermal impact and (b) non-isothermal impact on a sapphire-glass substrate and for a droplet temperature of 95 °C.

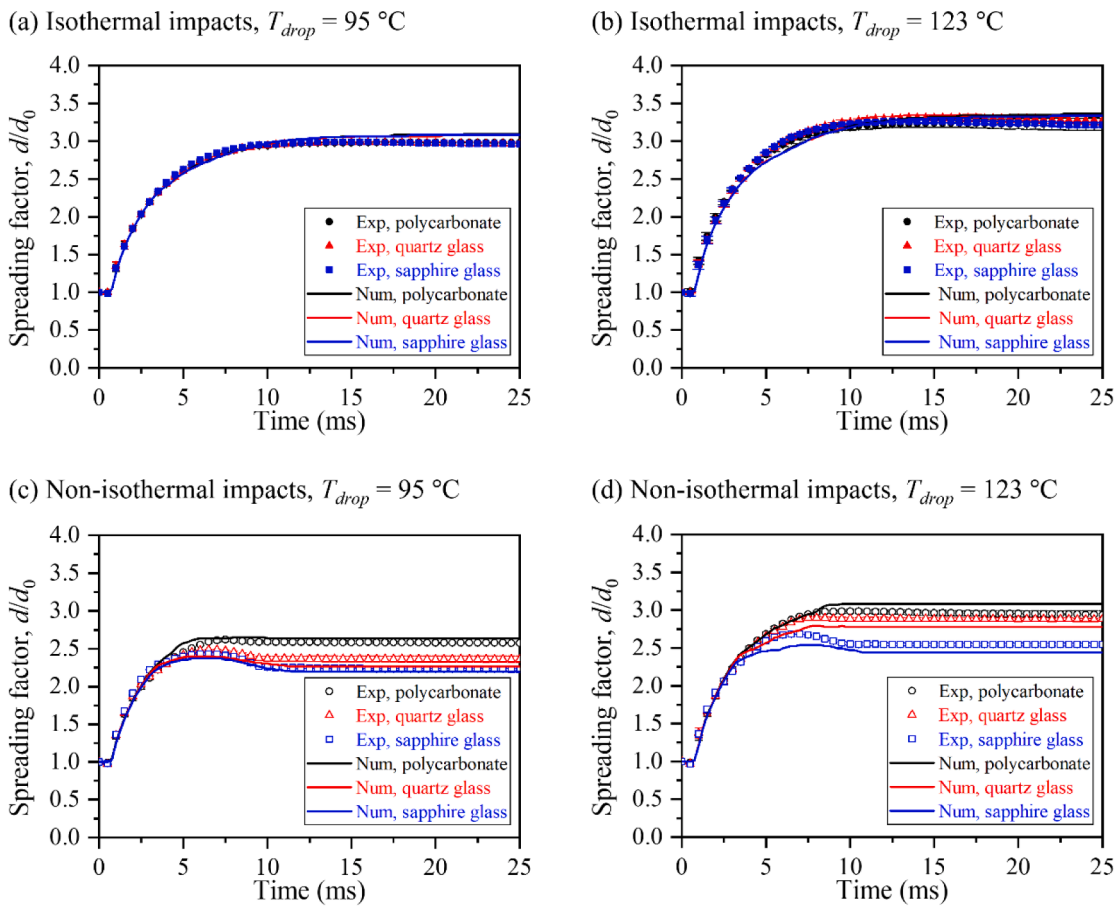

Fig. 14. Spreading factors of isothermal impact for droplet temperatures of (a) 95 °C and (b) 123 °C, and of non-isothermal impact at (c) 95 °C and (d) 123 °C.

secondary droplet was not intentionally reproduced in the simulation because it is not the focus of this study. The second droplet impacted the primary splat at around 30 ms, whereas our simulations mainly focused on droplet spreading during the initial 25 ms. A volume of the secondary droplet is less than 1 % of the primary droplet, thus it is believed to have very limited influence on the transient solidification at the interface.

After impact, the splats gradually solidified along with the heat transfer with the substrate and ambient environment. The experimental and numerical final geometries of the solidified splats after non-isothermal impacts are compared in Fig. 15 for droplet temperatures of (a) 95 °C and (b) 123 °C. Good agreement was observed between the simulation results and experimental measurements.

5.2. Solidification of the impacted droplets

For non-isothermal impact, the heat transfer and solidification occurred immediately after the impact at the bottom surface of the splats and significantly affected the spreading dynamics. Accurate simulation of this transient phenomenon is critical for predicting the non-isothermal impact of droplets. Fig. 16 shows the time evolution of the calculated thickness of the solidified layer at the splat center. Here, the solidified layer thickness (red line) is compared with the measured gray values (black open symbols in Fig. 16, which was also shown in Fig. 9) for the three substrates for a droplet temperature of 95 °C. Because the impacted droplet was black in liquid and gradually became white during solidification, the gray values serve as a parameter to quantify the degree of solidification. We speculate that a solid layer with certain thickness formed near the interface when the gray values became saturated. In Fig. 16, the gray value at $t = 100$ ms is termed G_{sat}, which refers to the gray value at saturation. t_{sat} represents the time when the gray values first reach G_{sat}. δ_{sat} is the calculated thickness of the solid layer at $t = t_{sat}$. The values of these three parameters are summarized in Table 6 for each substrate. G_{sat} is approximately 215 for all three substrates. For the polycarbonate substrate, the gray values became saturated at 71 ms. For the quartz-glass and sapphire-glass substrates, which had higher thermal conductivity, this process was much faster and the gray values reached saturation at 13 ms. The computed values of δ_{sat} were 23.5, 23.5, and 35.3 μm for impacts on polycarbonate, quartz-glass, and sapphire-glass substrates, respectively. Even though the polycarbonate substrate requires a much longer time for the gray values to reach saturation, similar solid-layer thickness were calculated for the three substrates. This suggests that the point of saturation of gray values might correspond to a specific solid-layer thickness for a given droplet material. Comparison of the measured gray values and calculated solid-layer thickness suggested that the simulation provides an accurate prediction of the transient solidification at the bottom surface of the splat immediately after impact.

We used the photographs of the impacted droplets during solidification to directly compare the simulation results with the experimental results in terms of the transient solidification at the interface. Figs. 17–19 present a comparison of the photographs and numerical results of the solidification at the bottom surface of the splat for impact on the three substrates. The photographs on the left present the gray values of the splat observed from the bottom. The images on the right side are computer-generated; the background of these images is black, which is the same as the photographs. The gray values of the splat were determined according to the calculated thickness of the solid layers. The splat was black before solidification and the gray values gradually increased to G_{sat} (i.e., 215 when the calculated thickness of the solid layer increased to typical sizes of 23.5 or 35.3 μm, depending on the

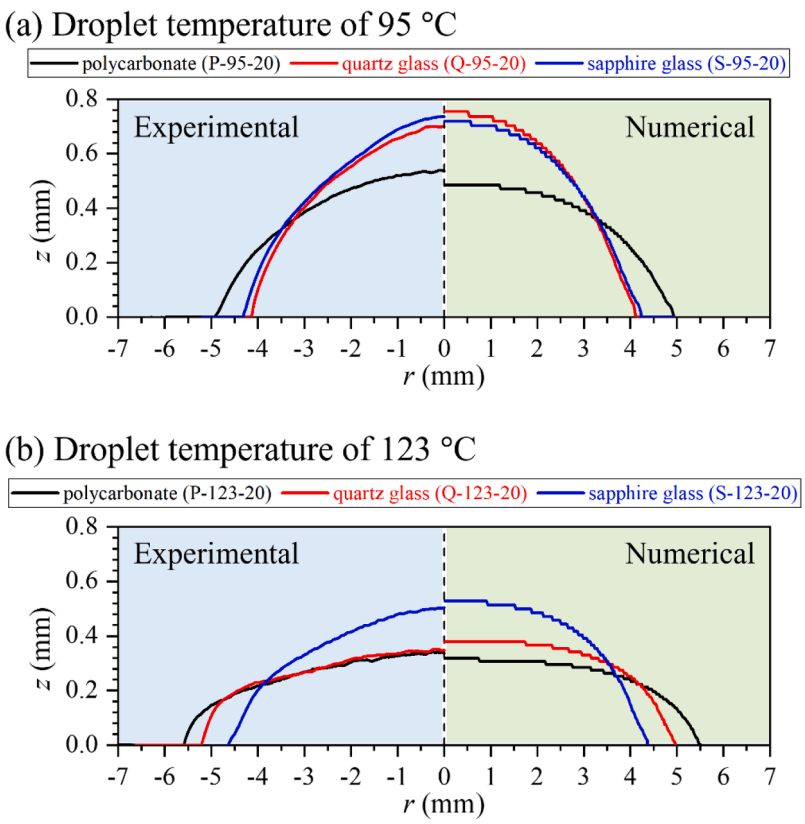

Fig. 15. Comparison of the numerical and experimental final geometries of the splats after solidification for droplet temperatures of (a) 95 °C and (b) 123 °C.

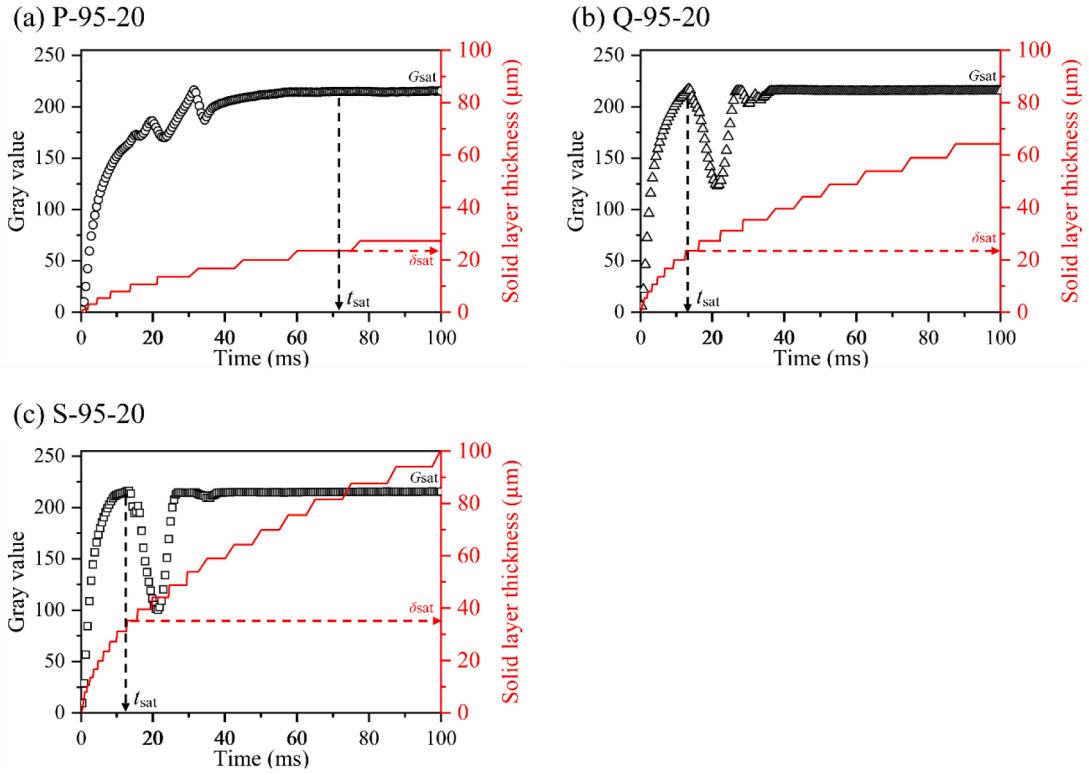

Fig. 16. Time evolution of the calculated thickness of the solid layer at the splat center and the measured gray values for non-isothermal impact on three types of substrates for a droplet temperature of 95 °C.

Table 6
Typical parameters for identifying gray values and solid-layer thickness in Fig. 16.

Testing No.	G_{sat}	t_{sat} (ms)	δ_{sat} (μm)
P-95-20	215.3	71	23.5
Q-95-20	215.3	13	23.5
S-95-20	215.5	13	35.3

substrate material). The gray values were assumed to linearly increase with the thickness of the solid layer. The simulation generally reproduced the solidification at the bottom surface of the splat for all conditions except for the bright ring at the splat periphery in certain photographs. This was caused by the refraction of the liquid piled up there (Fig. 3). The simulation results suggest that the gray values of the impacted droplets could be used as a parameter to evaluate the degree of initial transient solidification of impacted droplets. In addition, the good agreement between the numerical and experimental results suggests that the simulations provide accurate predictions of not only the initiation and progress of the solidification of an impacted droplet but also the subsequent dynamic behavior under various impact conditions.

5.3. *Effect of transient solidification on the spreading of impacted droplets*

To investigate the effect of transient solidification on the spreading of impacted droplets, the simulation results of the dimensionless contact radius, d_c/d_0, at the splat/substrate interface is plotted in Fig. 20(a) for impact of a 95 °C droplet on a polycarbonate substrate. The time evolutions of d_c/d_0 were compared for isothermal and non-isothermal impact. The volume ratio of the solid layer to the whole splat was termed V_s and its time evolution is plotted in Fig. 20(a) as the right axis. It can be seen that the contact line moved rapidly immediately after the impact and stopped expanding after several milliseconds. For non-isothermal impact, d_c/d_0 reached equilibrium much earlier than for isothermal impact because of transient heat transfer and solidification. The difference in d_c/d_0 between isothermal and non-isothermal impact increased with time owing to the progress of interface solidification. To quantitatively investigate the effect of solidification on the spreading of impacted droplets, the time at which the difference in d_c/d_0 between isothermal and non-isothermal impact reaches 3 % was termed $t^{0.03}$, which is shown in the enlarged graph (Fig. 20(b)). 3 % does not have a specific significance. This value was selected to quantify the effect of the transient solidification on droplet spreading, because we think that a

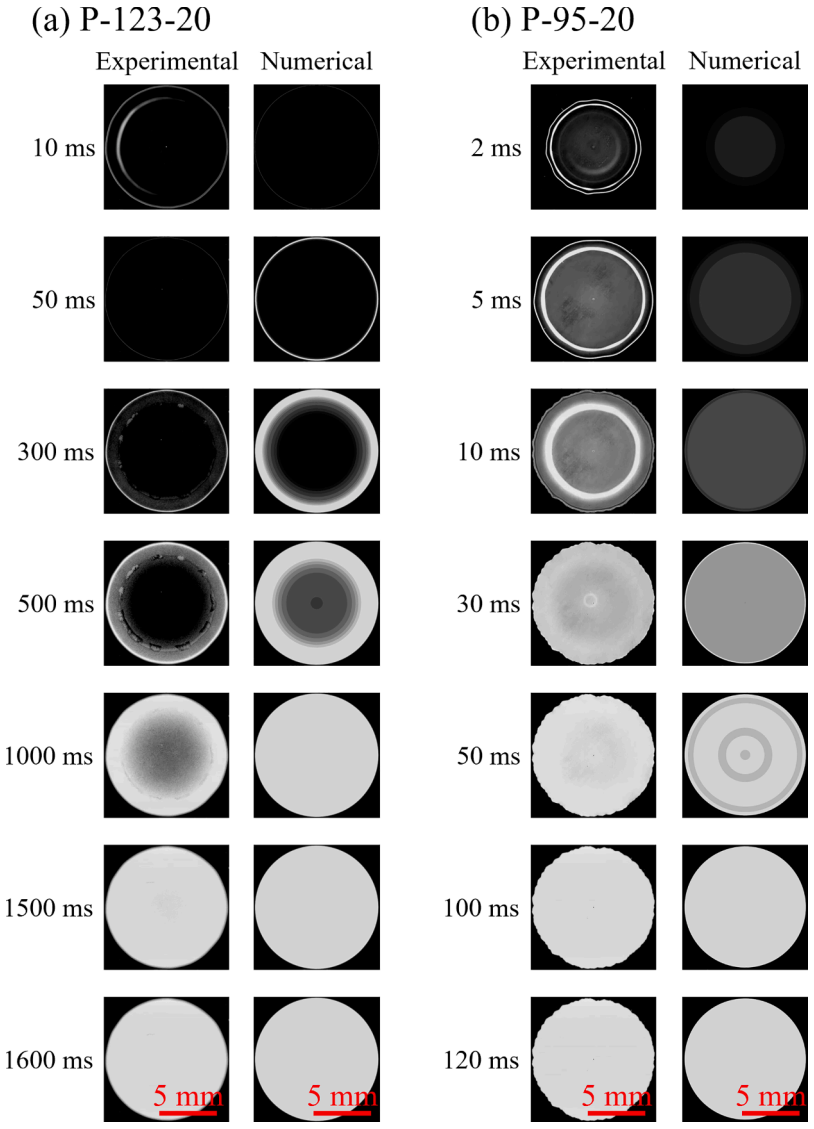

Fig. 17. Comparison of the experimental and numerical results of transient solidification at the bottom surface of the splat immediately after impact. The substrate material is polycarbonate. The droplet temperatures are (a) 123 °C and (b) 95 °C. The left panel displays photographs and the right panel displays computer-generated images, in which the gray values indicate the thickness of the solid layers.

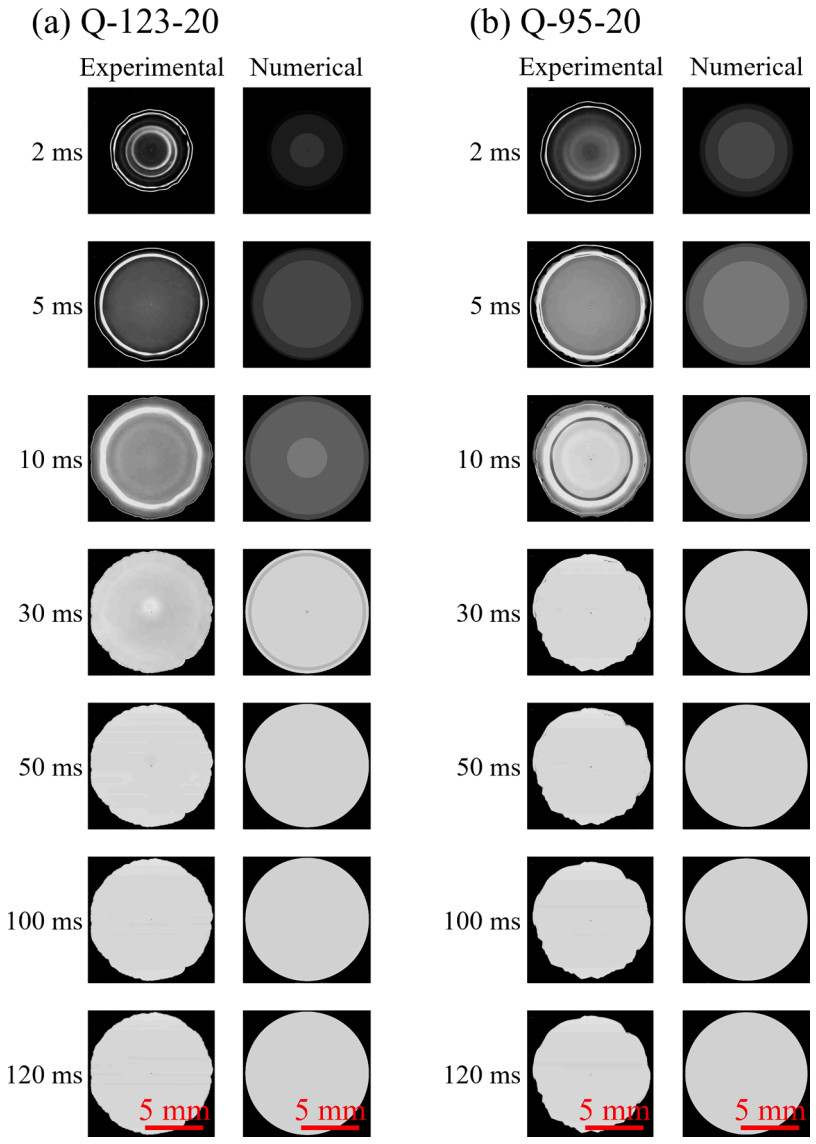

Fig. 18. Comparison of the experimental and numerical results of transient solidification at the bottom surface of the splat immediately after impact. The substrate material is quartz glass. The droplet temperatures are (a) 123 °C and (b) 95 °C.

difference of 3 % is sufficiently notable in terms of d_c/d_0. $t^{0.03}$ indicates the time when the spreading of the impacted droplet is first noticeably affected by transient solidification. Before this time, the inertial force dominates the fluid flow owing to the large kinetic energy and low level of solidification. The volume ratio of the solid layer at $t^{0.03}$ was termed $V_s^{0.03}$. $t^{0.03}$ and $V_s^{0.03}$ were calculated for each substrate and summarized in Table 7. It can be seen that a smaller $t^{0.03}$ is obtained for substrates with higher thermal conductivity. This suggests that transient solidification has a more pronounced effect on the spreading of the impacted droplets when the substrate has a higher thermal conductivity. In contrast with the large disparity in $t_{0.03}$, the values of V_s were much closer for the different substrates, ranging from 1.3 % to 1.8 %. This suggests that transient solidification starts to affect the spreading of impacted droplets at a low volumetric solid ratio. Furthermore, we speculate that transient solidification may have a comparable influence on the spreading of impacted droplets regardless of the impact conditions, as long as the degree of splat solidification is constant.

All the simulation results demonstrated that, although there are no direct correlations between the measured gray scales of impacted droplets and solid-layer thickness, the simulation yielded reasonable predictions for the spreading and transient solidification of the impacted molten droplets. Furthermore, the proposed experimental and numerical methods provide valuable guidance for studying droplet-impact problems, especially those involving transient solidification.

6. Conclusions

The spreading dynamics and transient solidification of paraffin droplets impacting solid surfaces were observed and numerically modeled. The effects of the substrate material, droplet temperature, and substrate temperature were thoroughly discussed. The impact behavior, including flattening and recoil, was observed from a horizontal view. The transient solidification at the bottom surface of the impacted droplet was observed through a mirror equipped below the transparent substrates. Numerical simulations were performed to model the whole impact behavior, including the impact, heat transfer, and solidification. The numerical results of the impact behavior were compared with the experimental results using several parameters, such as the spreading factor, dimensionless recoil height, geometry of the solidified splat, and thickness of the solid layer. The main results were drawn as follows.

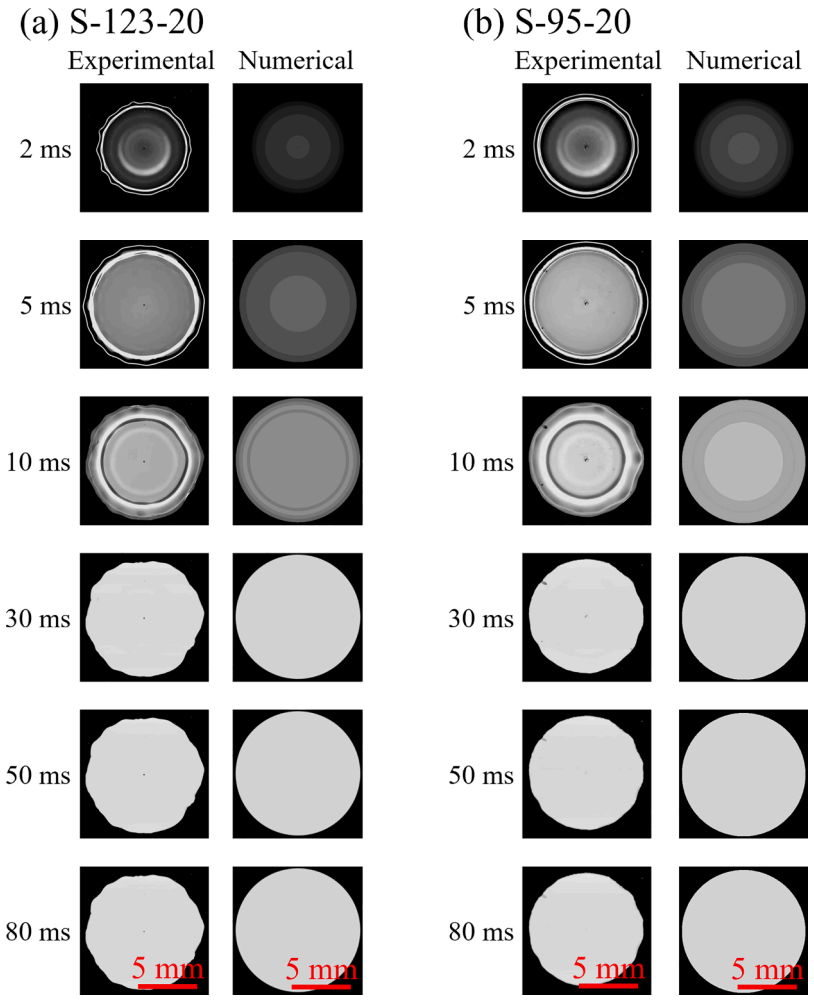

Fig. 19. Comparison of the experimental and numerical results of transient solidification at the bottom surface of the splat immediately after impact. The substrate material is sapphire glass. The droplet temperatures are (a) 123 °C and (b) 95 °C.

1. The substrate material has little effect on isothermal impact. In contrast, the thermal conductivity of the substrate material influences non-isothermal impact. A larger spreading factor and less-intense recoil were observed for droplet impact on the low-thermal-conductivity polycarbonate substrate. In addition, splat solidification initiated and progressed more slowly at the bottom surface for the polycarbonate substrate.
2. Two patterns of splat solidification were observed for non-isothermal impact. When the 123°C droplet impacted the polycarbonate substrate, the solidification initiated at the periphery and slowly progressed to the splat center. When the droplet temperature decreased to 95°C or the substrate materials changed to high-thermal-conductivity quartz glass and sapphire glass, the splat solidified rapidly and simultaneously across the entire bottom surface of the splat. The different patterns of splat solidification were caused by substrate thermal conductivities and temperature differences between the initial droplet temperature and its melting point.
3. The simulation results agree well with the experimental observations of the whole impact and spreading phenomena, as well as the transient solidification at the bottom surface of the splat. The observed gray values of the splat reached saturation at times ranging from 10 to 10^3 ms, depending on the impact conditions. The calculated solid-layer thickness at the time of saturation of the gray values was approximately constant, with a value of around 30 μm, regardless of the impact conditions. This suggests that the point of saturation of gray values might correspond to a specific solid-layer thickness with a given droplet material.
4. The effect of transient solidification on the spreading of impacted droplets was investigated using the parameter $V_s^{0.03}$. This refers to the volume ratio of the solid layer at a specific time ($t_{0.03}$) when the droplet flow is discernibly affected by the transient solidification. It was found that transient solidification had a more pronounced effect on the spreading of impacted droplets on substrates with higher thermal conductivity. Furthermore, transient solidification affected the spreading of impacted droplets with a low level of splat solidification when the volumetric ratio of the solid layer was less than 2 %.

CRediT authorship contribution statement

Chao Kang: Conceptualization, Methodology, Software, Validation, Formal analysis, Investigation, Data curation, Writing – original draft, Writing – review & editing, Visualization. **Ikki Ikeda:** Conceptualization, Methodology, Software, Validation, Formal analysis, Investigation, Data curation. **Motoki Sakaguchi:** Conceptualization, Methodology, Software, Validation, Resources, Writing – review & editing, Visualization, Supervision, Project administration, Funding acquisition.

Declaration of competing interest

The authors declare that they have no known competing financial

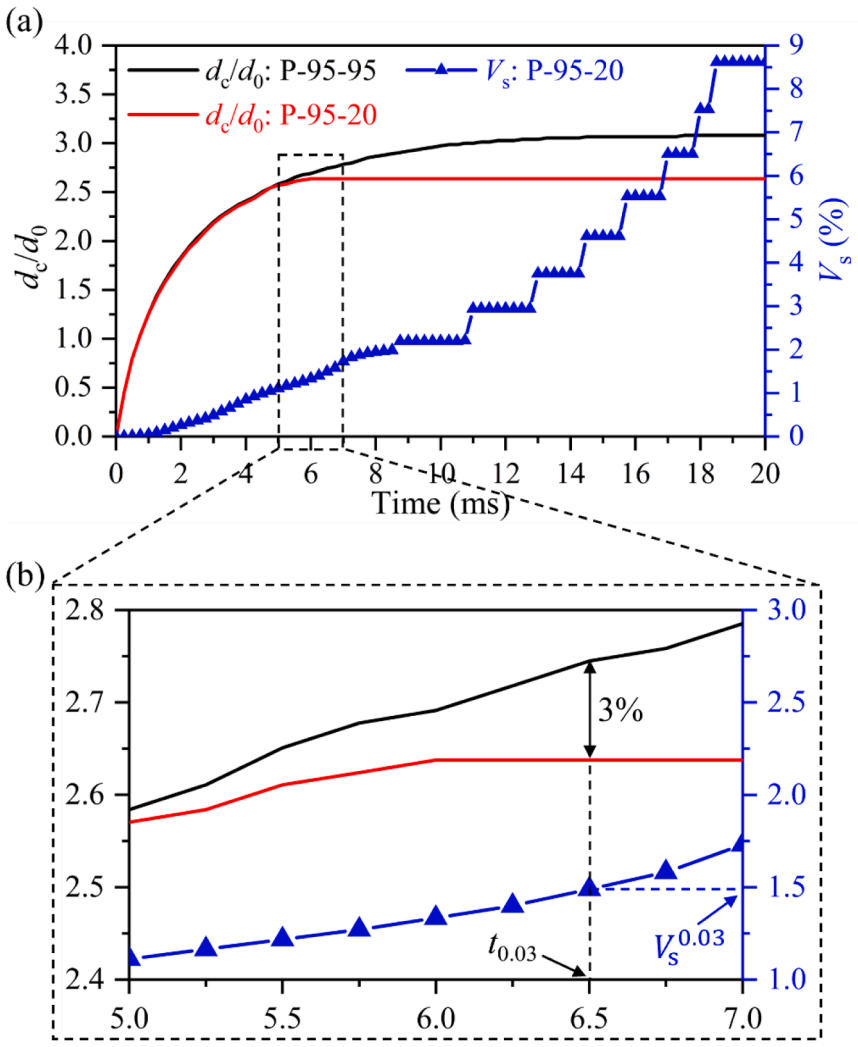

Fig. 20. (a) Comparison of the time evolutions of d_c/d_0 under isothermal and non-isothermal impact, and the volume ratio of the solid layer to the whole splat. (b) Enlarged graph to show the definitions of $t^{0.03}$ and $V_s^{0.03}$.

Table 7
$t^{0.03}$ and $V_s^{0.03}$ for each substrate.

Testing No.	$t^{0.03}$ (ms)	$V_s^{0.03}$ (%)
P-95-20	6.5	1.5
Q-95-20	3.8	1.8
S-95-20	2.3	1.3

interests or personal relationships that could have appeared to influence the work reported in this paper.

Data availability

Data will be made available on request.

Acknowledgment

This work was supported by JSPS KAKENHI Grant-in-Aid for Scientific Research (B) 21H01206. We thank Adam Brotchie, PhD, from Edanz (https://jp.edanz.com/ac) for editing a draft of this manuscript.

References

[1] S. Chandra, P. Fauchais, Formation of solid splats during thermal spray deposition, J. Therm. Spray Technol. 18 (2) (2009) 148–180, https://doi.org/10.1007/s11666-009-9294-5.
[2] H. Wijshoff, Drop dynamics in the inkjet printing process, Curr. Opin. Colloid Interface Sci. 36 (2018) 20–27, https://doi.org/10.1016/j.cocis.2017.11.004.
[3] H. Yi, J. Li, Z. Wang, H. Cao, M. Liu, Elimination of gas entrapment in droplet-based 3D printing by induced electric-field, Int. J. Mech. Sci. 266 (2024) 108974, https://doi.org/10.1016/j.ijmecsci.2024.108974.
[4] M. Tembely, R. Attarzadeh, A. Dolatabadi, On the numerical modeling of supercooled micro–droplet impact and freezing on superhydrophobic surfaces, Int. J. Heat Mass Transf. 127 (2018) 193–202, https://doi.org/10.1016/j.ijheatmasstransfer.2018.06.104.
[5] C. Josserand, S.T. Thoroddsen, Drop impact on a solid surface, Annu. Rev. Fluid Mech. 48 (2016) 365–391, https://doi.org/10.1146/annurev-fluid-122414-034401.
[6] R. Rioboo, M. Marengo, C. Tropea, Time evolution of liquid drop impact onto solid, dry surfaces, Exp. Fluids 33 (2002) 112–124, https://doi.org/10.1007/s00348-002-0431-x.
[7] H. Almohammadi, A. Amirfazli, Droplet impact: Viscosity and wettability effects on splashing, J. Colloid Interface Sci. 553 (2019) 22–30, https://doi.org/10.1016/j.jcis.2019.05.101.
[8] Y. Guan, J. Fu, S. Wu, X. Chen, C. Zhou, The post–impact dynamics of drop rebound on inclined hydrophobic surfaces of various wettabilities, Phys. Fluids 33 (2021) 072108, https://doi.org/10.1063/5.0048805.
[9] G. Liang, I. Mudawar, Review of drop impact on heated walls, Int. J. Heat Mass Transf. 106 (2017) 103–126, https://doi.org/10.1016/j.ijheatmasstransfer.2016.10.031.
[10] C. Kang, M. Sakaguchi, A. Amano, Y. Kurokawa, H. Inoue, Quenching stress and fracture of paraffin droplet during solidification and adhesion on metallic

substrate, Surf. Coat. Technol. 374 (2019) 868–877, https://doi.org/10.1016/j.surfcoat.2019.06.067.
[11] D. Jia, D. Zhou, P. Yi, C. Zhang, J. Li, Y. Guo, S. Zhang, Y. Li, Splat deposition stress formation mechanism of droplets impacting onto texture, Int. J. Mech. Sci. (2024) 109002, https://doi.org/10.1016/j.ijmecsci.2024.109002.
[12] Y. Okajima, M. Sakaguchi, H. Inoue, A finite element assessment of influential factors in evaluating interfacial fracture toughness of thermal barrier coating, Surf. Coatings Technol. 313 (2017) 184–190, https://doi.org/10.1016/j.surfcoat.2017.01.052.
[13] C. Kang, M. Sakaguchi, A. Saito, H. Inoue, Adhesion strength of paraffin droplet impacted and solidified on metal substrate, Results Phys. 34 (2022) 105310, https://doi.org/10.1016/j.rinp.2022.105310.
[14] W.Z. Fang, F. Zhu, L. Zhu, W.Q. Tao, C. Yang, Self-peeling of frozen water droplets upon impacting a cold surface, Commun. Phys. 5 (1) (2022) 51, https://doi.org/10.1038/s42005-022-00827-0.
[15] J.Y. Kim, K. Cho, S.A. Ryu, S.Y. Kim, B.M. Weon, Crack formation and prevention in colloidal drops, Sci. Rep. 5 (2015) 1–9, https://doi.org/10.1038/srep13166.
[16] C. Kang, I. Ikeda, M. Sakaguchi, Recoil and solidification of a paraffin droplet impacted on a metal substrate: Numerical study and experimental verification, J. Fluids Struct. 118 (2023) 103839, https://doi.org/10.1016/j.jfluidstructs.2023.103839.
[17] K. Fukudome, Y. Muto, K. Yamamoto, H. Mamori, M. Yamamoto, Numerical simulation of the solidification phenomena of single molten droplets impinging on non–isothermal flat plate using explicit moving particle simulation method, Int. J. Heat Mass Transf. 180 (2021) 121810, https://doi.org/10.1016/j.ijheatmasstransfer.2021.121810.
[18] C. Shinan, D. Liang, S. Mengjie, L. Mengyao, Numerical investigation on impingement dynamics and freezing performance of micrometer–sized water droplet on dry flat surface in supercooled environment, Int. J. Multiph. Flow 118 (2019) 150–164, https://doi.org/10.1016/j.ijmultiphaseflow.2019.06.011.
[19] C.H. Wang, H.L. Tsai, Y.C. Wu, W.S. Hwang, Investigation of molten metal droplet deposition and solidification for 3D printing techniques, J. Micromech. Microeng. 26 (2016) 095012, https://doi.org/10.1088/0960-1317/26/9/095012.
[20] C.Le Bot, S. Vincent, E. Meillot, F. Sarret, J.P. Caltagirone, L. Bianchi, Numerical simulation of several impacting ceramic droplets with liquid/solid phase change, Surf. Coat. Technol. 268 (2015) 272–277, https://doi.org/10.1016/j.surfcoat.2014.10.047.
[21] L. Xia, F. Chen, T. Liu, D. Zhang, Y. Tian, D. Zhang, Phase-field simulations of droplet impact on superhydrophobic surfaces, Int. J. Mech. Sci. 240 (2023) 107957, https://doi.org/10.1016/j.ijmecsci.2022.107957.
[22] Y. Zhang, S. Matthews, D. Wu, Y. Zou, Interactions between successive high-velocity impact droplets during plasma spraying, Surf. Coat. Technol. 431 (2022) 128006, https://doi.org/10.1016/j.surfcoat.2021.128006.
[23] J. Huang, L. Qi, J. Luo, Q. Wang, A study on the solidification shapes of molten metal droplet impacting at low weber number, Phys. Fluids 35 (2023) 092102, https://doi.org/10.1063/5.0165888.
[24] S. Haferl, D. Poulikakos, Experimental investigation of the transient impact fluid dynamics and solidification of a molten microdroplet pile–up, Int. J. Heat Mass Transf. 46 (2003) 535–550, https://doi.org/10.1016/S0017-9310(02)00289-2.
[25] M.V. Gielen, R. de Ruiter, R.B.J. Koldeweij, D. Lohse, J.H. Snoeijer, H. Gelderblom, Solidification of liquid metal drops during impact, J. Fluid Mech. 883 (2020) A32, https://doi.org/10.1017/jfm.2019.886.
[26] Y. Zhang, S. Matthews, P. Munroe, M. Hyland, Plasma-sprayed nickel splats on chromium substrates: The role of substrate preheating and thermal conductivity, Appl. Surf. Sci. 494 (2019) 124–136, https://doi.org/10.1016/j.apsusc.2019.06.266.
[27] Y. Zhang, S. Matthews, M. Hyland, Role of solidification in the formation of plasma sprayed nickel splats through simulation and experimental observation, Int. J. Heat Mass Transf. 115 (2017) 488–501, https://doi.org/10.1016/j.ijheatmasstransfer.2017.07.072.
[28] W.Z. Fang, F.Q. Zhu, F. Shen, D. Chai, W.Q. Tao, Freezing behaviors of impacting water droplets on cold inclined surfaces, Appl. Therm. Eng. 219 (2023) 119562, https://doi.org/10.1016/j.applthermaleng.2022.119562.
[29] W.Z. Fang, F. Zhu, W.Q. Tao, C. Yang, How different freezing morphologies of impacting droplets form, J. Colloid Interface Sci. 584 (2021) 403–410, https://doi.org/10.1016/j.jcis.2020.09.119.
[30] P. Chantelot, D. Lohse, Drop impact on superheated surfaces: From capillary dominance to nonlinear advection dominance, J. Fluid Mech. 963 (2023) 1–14, https://doi.org/10.1017/jfm.2023.290.
[31] G. Castanet, W. Chaze, O. Caballina, R. Collignon, F. Lemoine, Transient evolution of the heat transfer and the vapor film thickness at the drop impact in the regime of film boiling, Phys. Fluids 30 (2018) 122109, https://doi.org/10.1063/1.5059388.
[32] T. Tran, H.J.J. Staat, A. Prosperetti, C. Sun, D. Lohse, Drop impact on superheated surfaces, Phys. Rev. Lett. 108 (2012) 1–5, https://doi.org/10.1103/PhysRevLett.108.036101.
[33] M.Sakaguchi Amano, Y. Kurokawa, Y. Okajima, H. Inoue, Measurement of quenching strain in paraffin drop test modelling thermal spray process, Trans. JSME 83 (2017) 1–14, https://doi.org/10.1299/transjsme.17-00377 (in Janpanse).
[34] M.Sakaguchi Kang, H. Inoue, Contribution of creep to strain evolution in a paraffin droplet during and after rapid solidification on a metal substrate, Surf. Coat. Technol. 399 (2020) 126145, https://doi.org/10.1016/j.surfcoat.2020.126145.
[35] H. Dong, W.W. Carr, J.F. Morris, An experimental study of drop–on–demand drop formation, Phys. Fluids 18 (2006) 072102, https://doi.org/10.1063/1.2217929.
[36] C.W. Hirt, B.D. Nichols, Volume of fluid (VOF) method for the dynamics of free boundaries, J. Comput. Phys. 39 (1981) 201–225, https://doi.org/10.1016/0021-9991(81)90145-5.